Optimization of a Dipole with Partially Keystoned Cable for the SIS 300

I. Bogdanov, S. Kozub, P. Shcherbakov, L. Tkachenko, V. Zubko, C. Muehle, G. Moritz, D. Tommasini

***Abstract*-- The last stage of the GSI Fast-Pulsed Synchrotron Project for FAIR (Facility for Antiproton and Ion Research) is the SIS 300 ring, which will use superconducting dipoles with 100 mm aperture, 6 T magnetic field amplitude and 1 T/s field ramp rate. Stringent requirements on physical parameters and on the dependable service of the dipole necessitated using a cable with increased current carrying capability and low dynamic losses. A suitable geometry of the superconducting cable was found in that used for the outer layer of the Large Hadron Collider superconducting main dipole, supplemented by a stainless steel core for the reduction of the transverse contact resistance between the strands. The shape of the partially keystoned cable demands numerical methods for the optimization of the geometry in adaptation to the wide aperture dipole. The main characteristics of the optimized 2D and 3D geometry of the dipole are presented. Two grades of iron yoke steel were analyzed for use, in view of their resulting field quality. Thermal analysis of the dipole was carried out.**

***Index Terms*-- AC Losses; Magnetic Fields; Ramp Rate; Superconducting Magnets.**

I. Introduction

After consideration of the geometry of superconducting (SC) dipole design with 80 mm aperture for creation of fast-cycling magnetic fields [1], the aperture of the coil was increased to 100 mm. This wider aperture geometry required another analysis and new approaches for selection of a new design. Three new geometries with different thicknesses of collars were considered [2] with the aim of selecting the best variant, which would possess good field quality, minimal AC losses, and design reliability. After this analysis, the geometry with 30-mm collar thickness was chosen. These collars are intended to support the coil during magnet assembly and cool-down. The iron yoke and outer stainless steel shell will restrain the magnetic forces during magnet ramp-up. This geometry with 0.65-mm wire diameter Rutherford cables [2] satisfies all requirements but has ~0.5 K temperature margin. To increase this value up to 1 K, a new cable design with 0.825 mm strands was chosen. A partially keystoned cable was selected, to avoid critical current degradation due to cable keystoning.

Another aim of this work was to select the most suitable grade of steel for the magnet yoke. The magnetic properties of several steels were studied [3]. Two candidate steels (Fig. 1), 2212 and M250-50 were chosen for analysis of the influence of these steels on field quality, as well as on heat loss in the iron yoke during magnet pulsed operation.

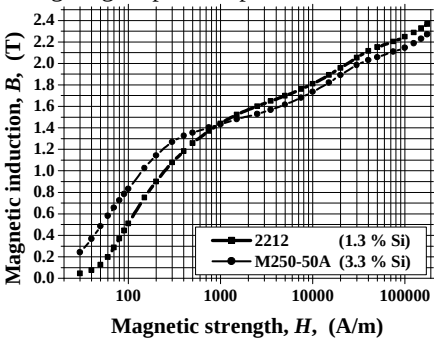

Fig. 1. BH data for two candidate steels for the magnet yoke

II. Characteristics of SC Strand and Cable

The original design consisted of a 0.825 mm diameter strand with 3.5-μm filaments of Nb47%Ti alloy, enclosed in a Cu matrix. The strand twist pitch was 5 mm and Cu/SC ratio was 1.4. The critical current density specification was not less then 2.7 kA/mm^2 at 5 T and 4.2 K. The following design calculations have been made with this wire specification.

Calculations showed that a temperature margin of ~1 K could be reached with a 36 strand cable. In order to save development time and costs, the geometry of the existing LHC dipole outer layer cable was adopted [4]. There is an essential difference, however: the new cable will contain a 25-μm stainless steel core, to decrease cable interstrand losses, arising in the cable during energizing/de-energizing of the magnet. The main geometric dimensions of the cable are (in mm):

Manuscript received September 18, 2005.

I. Bogdanov is with Institute for High Energy Physics (IHEP), Protvino, Moscow region, Russia, 142281 (e-mail: Igor.Bogdanov@ihep.ru).

S. Kozub is with Institute for High Energy Physics (IHEP), Protvino, Moscow region, Russia, 142281 (e-mail: Sergey.Kozub@ihep.ru).

P. Shcherbakov is with Institute for High Energy Physics (IHEP), Protvino, Moscow region, Russia, 142281 (e-mail: Petr.Shcherbakov@ihep.ru).

L. Tkachenko (corresponding author) is with Institute for High Energy Physics (IHEP), Protvino, Moscow region, Russia, 142281 (telephone: 7(0967)713223, e-mail: Leonid.Tkachenko@mail.ihep.ru).

V. Zubko is with Institute for High Energy Physics (IHEP), Protvino, Moscow region, Russia, 142281 (e-mail: Vasily.Zubko@ihep.ru).

C. Muehle is with Gesellschaft für Schwerionenforschung (GSI), Darmstadt, Germany (e-mail: C.Muehle@gsi.de).

G. Moritz is with Gesellschaft für Schwerionenforschung (GSI), Darmstadt, Germany (e-mail: G.Moritz@gsi.de).

D. Tommasini is with CERN, Geneva, Switzerland (e-mail: davide.tommasini@cern.ch).

Cable width with/without insulation	15.35/15.1
Cable minor thickness with/ without insulation	1.622/1.362
Cable major thickness with/ without insulation	1.858/1.598

The cable is insulated by 3 layers of polyimide film, with an effective cured insulation thickness of 125 μm in the radial direction and 95 μm in the azimuth direction.

III. 2D GEOMETRY

Mechanical calculations showed that the optimal thickness of the collars, needed for coil assembly, is 30 mm.

Placing of partially keystoned cable in the coil cross section creates a saw tooth curve at the inner and outer surfaces of the coil turn layers. In order to reduce the size of this saw tooth and to reach high field quality, each coil layer is divided into three blocks, as it is shown in Fig.2 (I quadrant).

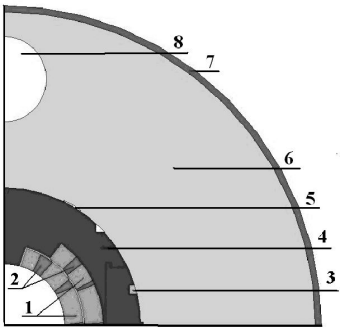

Fig. 2. Cross-section of dipole: 1–coil, 2-wedges, 3–key, 4–collars, 5–slot, 6–iron yoke, 7–stainless steel shell, 8-hole for II-phase helium.

Furthermore, the standard field representation will be used:

$$B_y + iB_x = B_0 \sum_{n=1}^{\infty} w_n(r,z)\left(\frac{r}{r_0}e^{i\theta}\right)^{n-1}, \mathrm{w_n} = \mathrm{b_n} + \mathrm{ia_n}.$$

Here, B_0 is the central field; r_0 = 40 mm is a reference radius, b_n and a_n are normal and skew field harmonics.

Calculations of magnetic field characteristics were made with the help of Roxie [5] and MULTIC [6] codes.

Variation of angular locations of six coil blocks allows one to suppress five lower field harmonics $b_3 - b_{11}$, giving a good field quality in the aperture. To reduce the load on the correction system as well, the following additional conditions were also imposed:

$$b_n^{(B)} = \int_{B\min}^{B\max} b_n(B)dB = 0; \quad \mathrm{n} = 3,5,7,9,11.$$

Here B_{min} = 1.6 T is the injection field and B_{max} = 6 T is the maximum central field during acceleration. Table I presents the main geometric parameters of the coil blocks.

TABLE I
MAIN GEOMETRIC PARAMETERS OF COIL BLOCKS

Block #	1	2	3	4	5	6
Turn number	17	11	7	18	9	9
R_i, mm	50.00	50.00	50.00	66.35	66.35	66.35
φ, deg.	0.12	33.61	61.30	0.67	26.24	43.08
α, deg.	7.60	38.37	64.43	4.50	28.15	44.98

Here φ is the initial angle of the coil block, α is its inclination angle, both from the median plane, and R_i is an inner radius of the layer.

Numerical simulations for optimization of the iron yoke geometry showed:

- Steel 2212 is better, from the viewpoint of field quality;
- There is an optimum thickness of iron $\Delta Fe = R_{outer} - R_{inner}$ at which it is possible to reduce $b_3^{(B)}$ close to zero.
- Decreasing ΔFe gives a negative growth in b_3; whereas increasing the radius of hole for II-phase helium r_h varies b_3 in positive direction. Therefore, it is possible to find a combination of values of ΔFe and r_h at which $b_3^{(B)} = 0$.

The relationship between optimum values of the parameters ΔFe and r_h is presented in Fig.3 for two steels.

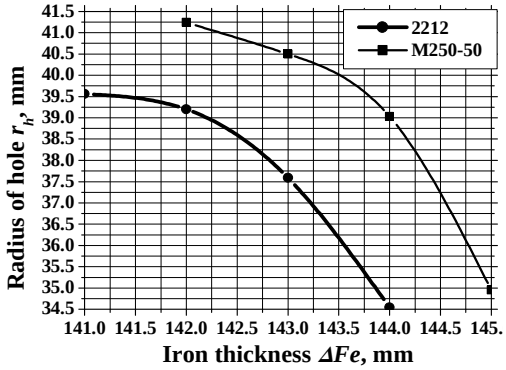

Fig. 3. Optimum parameters for suppressing $b_3^{(B)}$

For cryogenic reasons, the radius r_h must be close to 35 mm. A small rectangular slot is made on the inner surface of the iron to suppress $b_5^{(B)}$. The parameters for the optimum geometry of the iron yoke are given in Table II.

TABLE II.
GEOMETRIC OPTIMUM PARAMETERS OF IRON YOKE

Steel	2212	M250-50
Iron thickness, mm	143.5	144.5
Radius of hole, mm	35	35
Center of hole, mm	200.8	201.8
Angular position of slot, deg.	60	60
Depth of slot, mm	1	1
Angular size of slot, deg.	±3.6	±5.0

Dependences of transfer function and lower multipoles b_3 and b_5 versus central field are shown in Fig.4 and Fig.5 respectively, for the two previously mentioned steels. Multipoles b_7 and b_9 do not exceed 2×10^{-5} over the whole field range. Values of integrals $b_n^{(B)}$ are given in Table III. Maximum variations of the transfer function and multipoles b_3 and b_5 (peak-to-peak) are presented in Table IV.

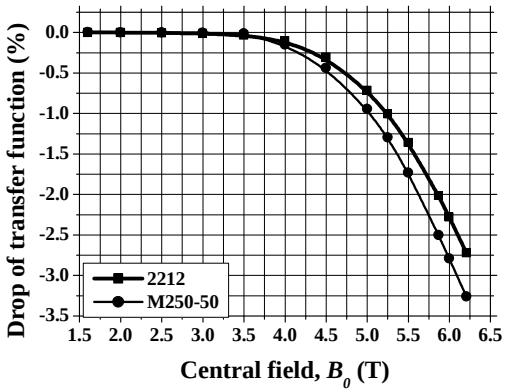

Fig. 4. Alteration of transfer function versus central field.

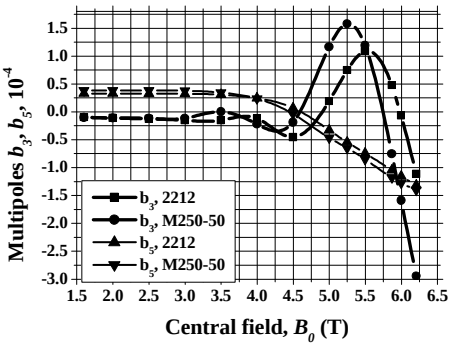

Fig. 5. Multipoles b_3 and b_5 versus central field.

TABLE III.
VALUES OF INTEGRALS $b_n^{(B)}$, 10^{-4}

n	2212	M250-50
3	-0.02	0.06
5	-0.11	-0.20
7	-0.26	-0.32
9	0.36	0.36

TABLE IV.
MAXIMUM VARIATIONS OF THE TRANSFER FUNCTION AND MULTIPOLES B_3 AND B_5 (PEAK-TO-PEAK)

	2212	M250-50
$\Delta(B/B_0)$, %	-2.3	-2.8
$\Delta\|b_3\|$, 10^{-4}	1.2	3.2
$\Delta\|b_5\|$, 10^{-4}	1.5	1.7

Values, presented in Figs. 4 – 5 and Tables III - IV, could be used for computer simulation of beam tracking. This allows one to formulate reasonable values of the multipoles, required for the correction systems, as well as to make the best choice of iron for the yoke. Other magnetic parameters have a weak dependence on material for the yoke (Table V).

TABLE V.
MAIN MAGNETIC PARAMETERS

Stored energy, kJ/m	256
Operating current, kA	6.29
Inductance, mH/m	12.9
Vertical force, kN/m	1316
Horizontal force, kN/m	-542
Total force, kN/m	1423

IV. 3D GEOMETRY

Decomposition of the integral field can be determined by integrating the field series over *z*:

$$\hat{B}_y + i\hat{B}_x = \hat{B}_0 \sum_{n=1}^{\infty} \hat{W}_n(r) \left(\frac{r}{r_0} e^{i\theta} \right)^{n-1},$$

$$\hat{B}_0 = \int_{-\infty}^{\infty} B_y(0,0,z)dz, \quad \hat{W}_n = \hat{b}_n + i\hat{a}_n = \int_{-\infty}^{\infty} w_n(z)dz.$$

Optimization of the 3D geometry consists of independent suppression of lower multipoles of edge fields, minimization of field in end parts of the coil to the level of the central cross section, and obtaining maximum magnetic length. In analogy with the optimization of the 2D geometry, an additional constraint is added:

$$\int_{B\min}^{B\max} \hat{b}_n(B)dB = 0, \quad n = 3,5,7.$$

In order to get the maximum magnetic length of the dipole, the three coil blocks of the outer layer contained minimum length end spacers. The outermost block of the inner layer was split into two blocks in the magnet end, with $n_1 + n_2 = 17$ turns. Positions of the last blocks of the inner (n_1) and outer layers were fixed to get equal longitudinal lengths of both layers. Locations of other blocks were used for optimisation of the magnet end geometry, with the aim of getting good field quality. The optimized positions of these blocks allow one to suppress the four lower integral multipoles $\hat{b}_3, \hat{b}_5, \hat{b}_7, \hat{b}_9$. In addition, the spacers in the inner layer decrease field enhancement in the end parts of the dipole. Fig.6 shows the dependences of two lower non-zero multipoles of integral field versus turn number n_1 in the first block of the inner layer for the infinite length of the iron yoke with $\mu = \infty$.

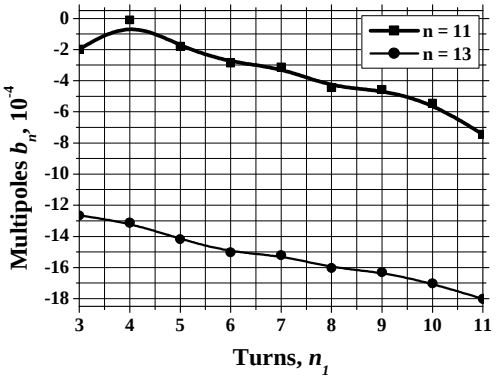

Fig. 6. Dependences of two lower non-zero multipoles of integral field versus turn number n_1 in the first block of the inner layer.

The required magnetic length of the dipole is equal to 2600 mm. Fig. 7 shows the necessary geometric length versus n_1 to attain this goal at infinite iron length with $\mu = \infty$.

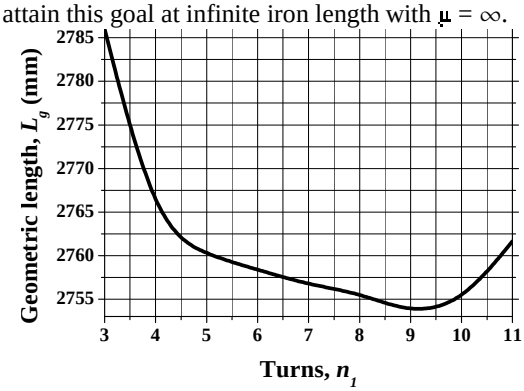

Fig. 7. Geometric length of dipole versus shifted number of turns.

Optimum geometry has to satisfy two conditions: minimum integral field multipoles and maximum magnetic length. Analysing Figs. 6-7, it can be seen that these conditions are best met with n_1 close to 5-8. For adjustment of the field enhancement in the end parts $B_{\max}^{(e)}$ to the level in the cross section ($B_{\max}^{(0)}$ = 6.421 T), it is necessary to shorten the length of the iron yoke. Dependence of maximum field in the end parts versus iron shortening ΔL_{Fe} is shown in Fig. 8 for n_1 = 5 - 8. These data are presented for 2212 steel.

Maximum integral field and magnetic length L_m are reached at $B_{\max}^{(e)} = B_{\max}^{(0)}$. Fig. 9 presents geometric length L_g for the required L_m = 2600 mm with optimum ΔL_{Fe} for different n_1 taken into account real dependence $\mu(B)$ in the iron yoke.

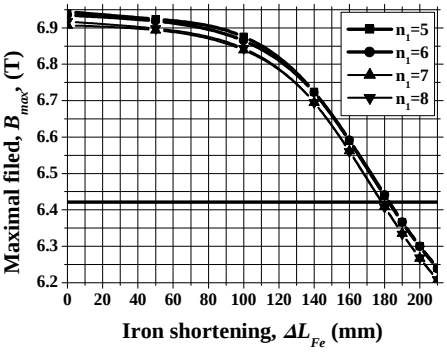

Fig. 8. Maximum field in the end parts versus iron shortening for different n_1. Horizontal line shows maximum field in the coil in the 2D cross- section.

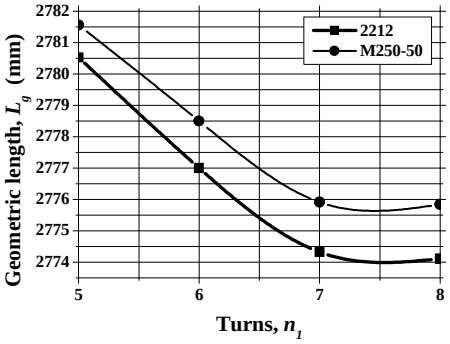

Fig. 9. Geometric length of the coil at L_m = 2600 mm versus n_1 for two steels.

Figs. 6-9 show that the optimum value of n_1 is 7. Fig. 4, 5 and 9 confirm that 2212 steel is better in comparison with M250-50 steel. The optimum parameters for the end parts (steel 2212) are n_1 = 7, ΔL_{Fe} = 178.5 mm, L_g = 2774.3 mm.

V. Losses and Temperatures

The AC losses in the coil are: hysteresis 41.9 J/m; matrix 14.1 J/m; cable 11.7 J/m and total 68.7 J/m. These values were calculated using crossover resistance R_c = 20 mΩ and adjacent resistance R_a = 200 μΩ. [7]. Heat losses in iron consist of hysteresis and eddy current losses. The latter are proportional to the square of the thickness of the laminated iron plates and can be suppressed to small values. Measured specific hysteresis losses w [3] can be described by

$$w = aB_{\max}^{b-1}\left(B_{\max} - B_{\min}\right) \text{ [mJ/kg].}$$

Here B_{max} and B_{min} are maximum and minimum fields in a volume element of iron. Table VI presents coefficients a and b and full hysteresis losses in iron for the two steels.

TABLE VI
COEFFICIENTS A, B AND HYSTERESIS LOSSES IN IRON

Steel	a	b	W, J/m
2212	10.507	2.360	44.8
M250-50	4.476	2.757	24.8

Preliminary calculations showed that the optimum cryogenic scheme of the accelerator ring consists of two strings with 60 dipoles in each string. The helium flow rate in circular channel is 38 g/s. Inlet temperature of helium in the first and last magnets are 4.40 and 4.61 K respectively. The magnet temperature margin is the difference between the critical and operating temperatures at the worst conditions of temperature, field and transport current. The calculations of temperature distribution in the coil versus time have been made for sequences of operating cycles. A difference between critical and operating temperatures for the I - IV quadrants, after several cycles for the inner layer of the last magnet in the string is presented in Fig.10.

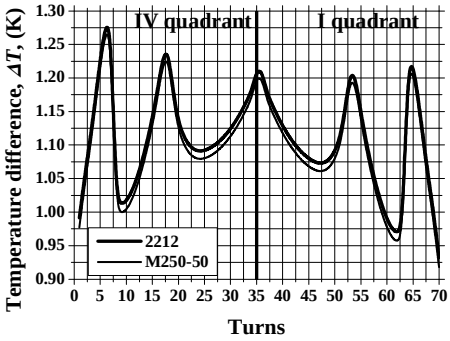

Fig. 10. Difference between critical and operating temperatures in turns in the I - IV quadrants of the inner layer for two steels.

The operating temperature is 4.763 K the critical temperature in the magnet is 5.695 K for 2212 steel and 5.681 K for M250-50, so the temperature margin is 0.932 K and 0.918 K respectively for the two kinds of steel.

VI. Conclusion

This work presents optimized 2D and 3D geometries for the SIS300 dipole. With such data, a magnet technical design could begin. The advantages in magnetic properties of 2212 steel, in comparison with M250-50 steel, are also shown. Additionally, in spite of lower losses in the magnet yoke with M250-50 steel, 2212 steel provides a higher temperature margin, thus ensuring better stability of the magnet.

VII. Acknowledgment

The authors wish to acknowledge B. Auchmann and S. Russenschuck, for their help in calculations with the CERN field computation program ROXIE and for useful and fruitful discussions.

References

[1] A. Ageev et al. “Development of Superconducting Dipole Design for Creation of Fast-Cycling Magnetic Fields.” Proc. of 18 Int. Conf. on Magnet Technology, Morioka, Japan, 2003. IEEE trans. on Appl. Sup., Vol. 14, Num. 2, pp.295-299.

[2] L. Tkachenko et al. “Comparison of three Designs of Wide Aperture Dipole for the SIS300 Ring.” European Particle Accelerator Conference EPAC’2004, Lucerne, Switzerland, 2004, pp.1747-1749.

[3] I. Bogdanov et al. “Study of Electrical Steel Magnetic Properties for Fast Cycling Magnets of SIS100 and SIS300 Rings.” European Particle Accelerator Conference EPAC’2004, Lucerne, Switzerland, 2004, pp. 1741-1743.

[4] “LHC Design Report”. CERN 2004-003. Vol. I, p.157.

[5] S. Russenschuk (Editor): “ROXIE: Routine for the Optimization of magnet X-sections, Inverse Field Calculation and Coil End Design”, First International ROXIE users meeting and workshop, 16-18.03.1998, — Proceedings. CERN 99-01. ISBN 92-9083-140-5.

[6] L.M. Tkachenko “Code Package MULTIC for Calculation of Magnetic Field with an Arbitrary Configuration”. IHEP preprint 92-28, 1992, (in Russian).

[7] M.N. Wilson et al. “Cored Rutherford Cables for the GSI Fast Ramping Synchrotron.” IEEE Trans. on V.13, Issue 2, June 2003 p.:1704 – 1709.